Isı Bilimi ve Tekniği Dergisi, 44, 1, 71-88, 2024
J. of Thermal Science and Technology
©2024 TIBTD Printed in Turkey
ISSN 1300-3615
e-ISSN 2667-7725
https://doi.org/10.47480/isibted.1494043

COMBINED FORCED AND NATURAL CONVECTION FROM A SINGLE TRIANGULAR CYLINDER

Zerrin Sert*
* Eskişehir Osmangazi University, School of Engineering and Architecture, Mechanical Engineering Department, 26480, Eskişehir/TURKEY, zbocu@ogu.edu.tr, ORCID: 0000-0001-6934-5443

(Geliş Tarihi: 04.05.2023, Kabul Tarihi: 05.12.2023)

Abstract: Unsteady laminar confined and unconfined fluid flow and mixed (forced and free) convection heat transfer around equilateral triangular cylinders are investigated numerically. The computation model is a two-dimensional domain with blockage ratios of BR=0.5, 0.25, 0.2, 0.1, 0.05, and 0.0333, with the Reynolds numbers ranging from 100 to 200. The working fluid is water (Pr = 7). The effects of aiding and opposing thermal buoyancy are incorporated into the Navier-Stokes equations using the Boussinesq approximation. The Richardson number, which is a relative measure of free convection, is varied in the range $-2 \leq Ri \leq 2$. The governing equations are solved by using the Finite Volume Method with a second-order upwind scheme used for differencing of the convection terms, and the SIMPLE algorithm is used for the velocity-pressure coupling. A discussion of the effect of the blockage ratio on the mean drag, mean rms lift coefficients, the Strouhal number, and the mean Nusselt number is also presented. The iso-vorticity contours and dimensionless temperature field are generated to interpret and understand the underlying physical mechanisms. The results reveal that, in addition to the Richardson and Reynolds numbers, the blockage rate is effective in the vortex distribution in the channel. It has been determined that the vortices formed behind the cylinder spread to the channel with a decreasing blockage rate. Especially at high Reynolds numbers, both the drag coefficient and the mean Nusselt number are significantly affected by the blockage ratio. For Ri=0, the drag coefficients for BR=0.25 in comparison to the BR=0.05 case are about 9% and 29% larger for Re= 100 and 200, respectively. For BR<0.1, two-column vortex formation at the back of the cylinder gave way to single vortexes in the aiding thermal buoyancy condition (Ri=2) compared to Ri=0 and -2. Also, useful correlations for flow characteristics and heat transfer are derived using the computed data.
Keywords: Heat transfer, Confined flow, Mixed convection, Equilateral triangle cylinder, Correlations.

TEK ÜÇGEN SİLİNDİRDEN TÜMLEŞİK ZORLANMIŞ VE DOĞAL TAŞINIM

Özet: Eşkenar üçgen silindir etrafında kararsız laminer sınırlı/sınırsız akışkan akışı ve tümleşik (doğal ve zorlanmış) taşınımla ısı transferi sayısal olarak incelenmiştir. Sayısal model, BR=0.5, 0.25, 0.2, 0.1, 0.05 ve 0.0333 blokaj oranlarına ve Reynolds sayılarının 100 ile 200 arasında değiştiği iki boyutlu bir alandır. Çalışma akışkanı sudur (Pr=7). Termal kaldırma kuvvetininin destek olma ve buna karşı çıkma etkileri, Boussinesq yaklaşımı kullanılarak Navier-Stokes denklemlerine dahil edilmiştir. Doğal taşınımın göreceli bir ölçüsü olan Richardson sayısı $2 \geq Ri \geq -2$ aralığında değişmiştir. Yönetici denklemler, taşınım terimlerinin ayrıklaştırılması için second order upwind şeması ile Sonlu Hacim Yöntemi kullanılarak çözülmüş ve hız-basınç bağlantısı için SIMPLE algoritması kullanılmıştır. Blokaj oranının ortalama sürükleme katsayısı, ortalama rms kaldırma katsayısı, Strouhal sayısı ve ortalama Nusselt sayısı üzerindeki etkisine ilişkin elde edilen sonuçlar çalışmada sunulmuştur. Eş girdap ve boyutsuz eş sıcaklık eğrileri altta yatan fiziksel mekanizmaları yorumlamak ve anlamak için oluşturulmuştur. Sonuçlar Richardson ve Reynolds sayılarına ek olarak blokaj oranının kanalda girdap dağılımında etkili olduğunu ortaya koymaktadır. Azalan blokaj oranı ile silindir arkasında oluşan girdapların kanala yayıldığı tespit edilmiştir. Özellikle yüksek Reynolds sayılarında hem sürükleme katsayısı hem de ortalama Nusselt sayısı blokaj oranından önemli ölçüde etkilendiği görülmüştür. Ri=0'da BR=0.25 için sürükleme katsayısı BR=0.05 durumuyla karşılaştırıldığında Re=100 ve 200'de sırasıyla yaklaşık %9 ve %29 daha yüksek çıkmıştır. BR<0.1 için Ri=0 ve -2'ye kıyasla termal kuvveti destekleyici durumda (Ri=2) kanal arkası çift girdap oluşumu yerini tekli girdaplara bırakmıştır. Ayrıca akış özellikleri ve ısı transferi için faydalı korelasyonlar, elde edilen veriler kullanılarak türetilmiştir.
Anahtar Kelimeler: Isı transferi, Sınırlı akış, Tümleşik taşınım, Eşkenar üçgen silindir, Korelasyonlar.

INTRODUCTION

The eddy shedding phenomenon behind the cylinder has been extensively studied by the fluid dynamics community because of its importance in engineering applications. Contrary to numerous publications on circular cylinders, it is only recently that research has been conducted on the forced flow over cylinders of different cross-sections (circular (Lupi, 2013; Laidoudi and Bouzit, 2018; Patel and Chhabra, 2019; Barati et al., 2022), square (Mahir and Altaç, 2019; Arif and Hasan, 2020; Sharma and Dutta, 2022), semicircular, elliptic (Zhang et al., 2020; Hyun and SikYoon, 2022; Salimipour and Yazdani, 2022), and trapezoidal). Although non-circular cylinders play a dominant role in many technical applications, there is very limited information in the literature on mixed (natural and force) convection heat transfer and flow over or from non-circular cylinders. Triangular cylinders can be used in different applications such as in the novel designs of heat exchangers (Tiwari and Chhabra, 2014), finned heat removal devices utilized as sinks in electronic cooling applications (Tiwari and Chhabra, 2014), polymer engineering applications (Laidoudi and Bouzit, 2018), and continuous thermal treatment of foodstuffs (Laidoudi and Bouzit, 2018), etc.

The 2-D numerical simulations of laminar flow around a triangular cylinder placed in free-stream (unconfined flow) were examined by De and Dalal (2006), Dulhani and Dalal (2015). Zeitoun et al. (2010) analyzed forced convection from a triangular cross-section in an unconfined channel for $Re=1.3\text{-}2\times10^5$. They found that the stream flows smoothly past the body with no separation at Re = 1.38 for their study. Zeitoun et al. (2011) examined 2-D laminar forced convection heat transfer around the horizontal triangular cylinder in the unconfined channel for $Re\leq200$ and Pr=0.71. They considered two configurations of the triangular cylinders: one when the vertex of the triangle faces the flow and the other when the base of the triangle faces the flow. They found the critical Reynolds number for both vertex-facing and the base-facing flows to be 38.03 and 34.7, respectively. Dhiman and Shyman (2011) examined the effects of Reynolds number on the heat transfer characteristics of a long (heated) equilateral triangular cylinder in the unconfined cross-flow regime for $50\leq Re \leq150$ and Pr=0.71. The fluid flow and mixed heat transfer around a triangular cylinder placed in an unconfined channel were examined numerically by Chatterjee and Mondal (2015). Their numerical simulations for combinations of Reynolds (Re=10-100), and Richardson (Ri=0-1) numbers are carried out for Pr=0.71. They reported that the amplitude of oscillation of the global flow and heat transfer quantities increased drastically, resulting from rapid mixing behind the obstacle. Altaç et al. (2019) investigated mixed convection heat transfer and fluid flow over a long horizontal equilateral triangular cylinder in an unconfined channel. Their simulation variables, Reynolds and Richardson numbers, are varied in the range $10 \leq Re \leq 200$ and $0 \leq Ri \leq 10$. Çelik and Altaç (2023) numerically investigated unsteady heat and fluid flow over a triangular cylinder with rounded corners. They considered a 2-D laminar regime ($50 \leq Re \leq 250$), two fluids (air and water), corner rounding, and cylinder orientation on the heat and flow characteristics. They reported that the mean Nusselt number (local heat transfer coefficient) for Pr = 0.7 and 7 is markedly influenced by the flow conditions and geometric orientations rather than corner rounding. However, in this study, the confined channel was handled, and the effects of the blockage ratio on heat transfer were examined.

The heat transfer and flow past a triangular cylinder in horizontal channels of $1/12 \leq BR \leq 1/3$ were numerically investigated by De and Dalal (2007) for $80 \leq Re \leq 200$. Srikanth et al. (2010) investigated the fluid flow and heat transfer across a long equilateral triangular cylinder placed in a confined channel for Re=1-80, Pr=0.71, and a blockage ratio of 0.25. They reported that the mean Nusselt number and the wake length increased with the increasing Reynolds number, and the average drag coefficient decreased with the increasing Reynolds number. Shademani et al. (2013) analyzed viscous and incompressible flow over an equilateral triangular obstacle placed in a confined horizontal channel (BR=0.05). They found the critical value of the Reynolds number ($Re \leq 38.03$). In reference (De and Dalal, 2007; Srikanth et al., 2010; Shademani et al., 2013), studies were performed for pure forced convection in the confined channel. Abbasi et al. (2001) examined the flow and heat transfer from a heated triangular cylinder in a 2D horizontal confined channel for Pr = 0.71, Grashof number ($0\leq Gr\leq1.5\times10^4$), and $20 \leq Re \leq 250$. Hassab et al. (2013) examined experimentally laminar mixed convection heat transfer from an isothermal horizontal triangular cylinder for Grashof numbers ranging from 26.32×10^4 to 213.46×10^4, Reynolds numbers ranging from 75.3 to 1251.6, and the attack angles from 0° to 180°. They concluded that whereas convection heat transfer increased with the angle of attack, conduction heat transfer remained constant with the Reynolds number. Additionally, they noted that for a given Reynolds number, the Nusselt number decreased as the airflow's attack angle increased. Rasool et al. (2015) examined the effects of mixed (natural and force) convection from a confined equilateral triangular cylinder placed centrally at an axis of a horizontal channel with a blockage ratio of 25% for Pr=0.71, Re=1-150, and Ri=0-2. Varma et al. (2015) studied mixed convective flow and heat transfer characteristics past a triangular cylinder placed symmetrically in a vertical channel with the blockage ratios BR=1/3, 1/4, and 1/6 for Re = 100 and $-1\leq Ri\leq1$. Dhiman (2016) studied the flow and heat transfer around a long equilateral triangular placed in a horizontal channel with a blockage ratio range of 0.1 to 0.5 for Re= 1-80. Zhu et al. (2020) numerically investigated the fluid flow around trapezoidal cylinders with various base length ratios in the confined channel (BR=0.05) for Re=150. They examined typical attack angles and the different base length ratios. Moreover, some information on the flow around a triangular

cylinder in the turbulent flow regime is presented in the literature. The considered problems have been solved both experimentally (Peng et al., 2008; Srigrarom and Koh, 2008; Akbari et al., 2021) and numerically (El-Wahed et al., 1993; Camarri et al. 2006; Chattopadhyay, 2007; Ali et al., 2011). Yagmur et al. (2017) examined experimentally and numerically the flow structures around an equilateral triangular cylinder using the Particle Image Velocimetry (PIV) technique and the Large Eddy Simulation (LES) turbulence model. Numerical analyses were examined at three different Reynolds numbers (Re=2.9×10^3, 5.8×10^3, and 1.16×10^4) to obtain the changes in the Strouhal numbers and drag coefficients. They found that the Strouhal numbers were nearly St=0.22 for PIV and LES at all Reynolds numbers, and it could be inferred that these values were independent of the Reynolds number.

The literature review shows that mixed (buoyant and forced) convection heat transfer and fluid flow over triangular cylinders have received very little attention; however, the results on forced convection have shown that the use of triangular cylinders increases heat transfer compared to circular and square cylinders (Bovand et al., 2015). The purpose of this research is to computationally investigate the effects of aiding and opposing thermal buoyancy on heat transfer and fluid flow from triangular cylinders in a confined and/or unconfined upward cross-flow. The numerical simulation results have been obtained for $100 \le \mathrm{Re} \le 200$ and for blockage ratios of BR= 0.5, 0.25, 0.2, 0.1, 0.05, and 0.0333. Water (Pr = 7) is the working fluid, and the Richardson number range examined is $-2 \le \mathrm{Ri} \le 2$. This study is especially unique in that it examines the effect of blockage ratio as well as aiding and opposing buoyant forces.

PHYSICAL PROBLEM AND MATHEMATICAL MODEL

A schematic of the two-dimensional computational domain with a triangular cylinder embedded in it is shown in Fig. 1. The working fluid is water (Pr=7). The equilateral triangular cylinder of side length *D* is located at a distance of 15*D* from the channel entrance, and the overall length of the channel is constant at 50*D* in all cases. The heat transfer and flow simulations are carried out for blockage ratios (BR=*D*/*H*) of 0.5, 0.25, 0.2, 0.1, 0.05, and 0.0333. Furthermore, the channel width in the unconfined channel is *H*=70*D*.

In the two-dimensional flow of an incompressible fluid subjected to buoyant forces, the dimensionless governing equations can be expressed by for (Mahir and Altaç, 2019),

Continuity equation:

$$\nabla \cdot \mathbf{u} = 0 \tag{1}$$

Momentum equations:

$$\frac{\partial \mathbf{u}}{\partial \tau} + \mathbf{u} \cdot \nabla \mathbf{u} = -\nabla P + \frac{1}{\mathrm{Re}} \nabla^2 \mathbf{u} - \mathbf{g}\, Ri\, \Theta \tag{2}$$

Energy equation:

$$\frac{\partial \Theta}{\partial \tau} + \mathbf{u} \cdot \nabla \Theta = \frac{1}{\mathrm{Re\,Pr}} \nabla^2 \Theta \tag{3}$$

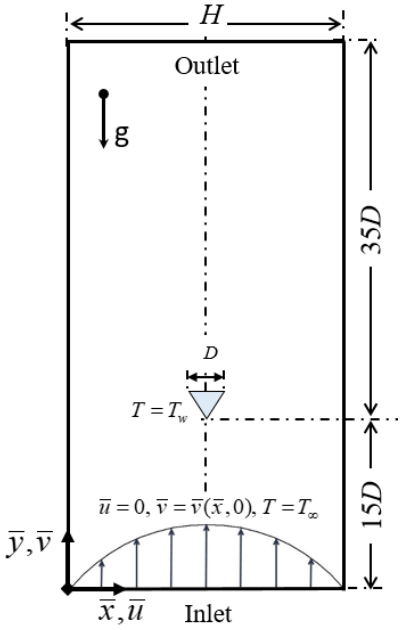

Figure 1. The schematic (dimensional) view of the applied geometry and computational domain.

where **u** is the dimensionless fluid velocity non-dimensionalized as $(\bar{u},\bar{v})/U_\infty$, τ is the dimensionless time defined as $\tau = U_\infty t/D$, t is time, x and y are the dimensionless coordinate variables in Cartesian coordinates non-dimensionalized as $(\bar{x},\bar{y})/D$, P is the pressure non dimensionalized by $\bar{P}/\rho U_\infty^2$, ρ is density of fluid, **g** is the dimensionless gravity defined by $(0,-1)^T$, Θ is the dimensionless temperature defined as $\Theta = (T - T_\infty)/(T_w - T_\infty)$, T is temperature, T_w and T_∞ are cylinder wall temperature and fluid inlet (or free stream) temperatures, respectively.

The boundary conditions used in the simulations are set as follows:

At the inlet:

For confined channel flows: The parabolic velocity profile defined by $u(x,0)=0$, $v(x,0) = 9\mathrm{BR} \cdot x(1 - x \cdot \mathrm{BR})$ for $1/70 \le \mathrm{BR} \le 1/2$, and $\Theta(x,0) = \Theta_\infty = 0$.

For unconfined channel flows: The fluid velocity and dimensionless temperature at the channel entrance are set $u(x,0) = 0$, $v(x,0) = 1$, and $\Theta(x,0) = \Theta_\infty = 0$.

On the left and right boundaries:

For confined channels: $u = 0,\ v = 0,\ \dfrac{\partial \Theta}{\partial y} = 0$

For unconfined channels: $u = 0,\ v = 1,\ \Theta_\infty = 0$

On the equilateral triangular cylinder walls:

$u = 0,\ v = 0,\ \Theta_w = 1$

At the outlet: $\dfrac{\partial u}{\partial x} = \dfrac{\partial v}{\partial x} = \dfrac{\partial \Theta}{\partial x} = 0$

An equilateral triangular cylinder is positioned along the centerline of the computational domain, and it is maintained at a constant isothermal temperature $(\Theta_w = 1)$.

The Boussinesq approximation is used to simulate the effect of aiding and opposing buoyant forces. The Richardson number defined as $\mathrm{Ri} = \mathrm{Gr}/\mathrm{Re}^2$ is varied in the range $-2 \le \mathrm{Ri} \le 2$. The mixed-convection configurations corresponding to the positive and negative values of the Richardson number, respectively, are assisting and opposing flow situations. In the heated cylinder ($\Theta_w > 0$), the buoyancy force assists forced convection (i.e., forced and free convection directions are upwards), while for a cooled cylinder case ($\Theta_w < 0$) the free convection is downwards in a direction that opposes the upwards forced convection.

The Reynolds, Grashof, and Prandtl numbers are defined as follows:

$$\mathrm{Re} = \frac{\bar{U}D}{\nu},\ \mathrm{Gr} = \frac{g\beta|T_w - T_\infty|D^3}{\nu^2},\ \mathrm{Pr} = \frac{\nu}{\alpha} \qquad (4)$$

where $\bar{U}$ is the mean velocity of the fluid at the channel inlet, ν is the kinematic viscosity, β is the thermal expansion coefficient, and α is the thermal diffusivity of the fluid. The side length D of the equilateral triangular cylinder is used to non-dimensionalize all geometrical lengths. The Reynolds numbers range from 100 to 200.

The mean Nusselt number over the whole cylinder surface is evaluated as follows:

$$\mathrm{Nu} = \frac{hD}{k} = \frac{1}{A_s}\int_{A_s} \mathrm{Nu}_s\, dA_s \qquad (5)$$

where h is the mean heat transfer coefficient, k is the thermal conductivity of the fluid, A_s is the cylinder wall surface area, $\mathrm{Nu}_s = -(\partial\Theta/\partial n)_s$ is the local Nusselt number computed as the dimensionless temperature gradient in the normal dimensionless direction (n) to the cylinder wall, and s represents the circulation distance along the perimeter of the triangular cylinder.

The drag and lift coefficients are defined as:

$$C_D = \frac{2F_D}{\rho D U_\infty^2},\quad C_L = \frac{2F_L}{\rho D U_\infty^2} \qquad (6)$$

where F_D and F_L are the drag and lift forces. The Strouhal number is defined as $St = fD/\bar{U}$ where $\bar{U}$ is the mean inlet velocity and f is the vortex shedding frequency.

NUMERICAL VALIDATION AND VERIFICATION

Numerical simulations in this study are carried out using the commercially available software ANSYS-Fluent®, where the continuity, momentum, and energy equations, Eqs. (1)-(3), are numerically solved by employing the finite volume method. The SIMPLE algorithm is used to solve the governing equations, and the second-order upwind differencing scheme is applied to discretize the equations. The convergence criterion for residuals is set to 10^{-5}.

The computational domain (unconfined channel, $70D \times 50D$) is meshed with non-uniform meshing using triangular elements (Gambit®). To determine the finest mesh, four alternative mesh structures with a wide range of nodes are used. G1, G2, G3, and G4 were established as grid alternatives. Table 1 shows the effects of the grid sensitivity on the cylinder surface mean Nusselt number (Nu), the mean drag coefficient ($C_{D,mean}$), and the Strouhal number for Re=100, Ri=0, Pr=0.7, and BR=0.1. The growth rate for the size of the triangular elements was 15% stretched out to the boundaries of the computational domain for G3. Moreover, an adaption procedure to the computation domain near the cylinder was employed. Due to yielding relative errors of 0.15% and 1.12%, respectively, for the mean Nusselt and $C_{D,mean}$ numbers, the G3 grid structure was selected for conducting numerical simulations of this study. Figure 2 shows a typical grid structure (G3) near the equilateral triangle.

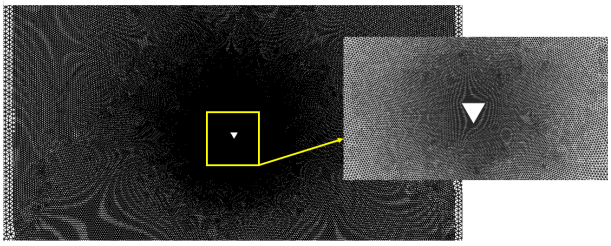

Figure 2. The grid structure of near the equilateral triangle.

The time step size in transient analysis also affects the accuracy of the numerical simulation. For this reason, the time step size is also varied to determine the optimum time step. The effect of varying the time step on the Nu, $C_{D,mean}$, and St is presented in Table 2 for the case of

Re=100, Ri=0, Pr=0.7, and BR=0.1. As a result, for subsequent simulations, the time step was chosen to be $\Delta\tau = 0.05$.

Table 1. The grid sensitivity for Re=100, Ri=0, Pr=0.7 and BR=0.1.

	G1	G2	G3	G4
Nodes Number	25952	57492	102986	410300
Cells Number	51082	113752	204328	817312
Nu	7.155	7.109	7.097	7.086
$C_{D,mean}$	0.858	0.878	0.886	0.896
St	0.3175	0.3125	0.3125	0.3125

According to the literature, a 2-D confined channel (BR=0.333) with an equilateral triangular cylinder is investigated at Ri=0 and Pr=0.7. The velocity at the inlet of this case is uniform. Table 3 depicts a comparison of the heat transfer and flow parameters for Re=100 and 150 with those available in the literature.

Table 2. The effects of time step size on heat and flow parameters for Re=100, Ri=0, Pr=0.7, and BR=0.1.

Time Step Size	Nu	$C_{D,mean}$	St
0.1	7.129	0.892	0.3223
0.075	7.109	0.888	0.3125
0.05	7.097	0.886	0.3125
0.025	7.091	0.886	0.3149

The comparison of the current pure convective computations reveals a good agreement in the cases of confined flow. The results for the mean drag coefficient, Nusselt and Strouhal numbers are quite consistent with those in the literature. Some minor discrepancies can be attributed to the selection of the size of the computational domain, gridding and near wall meshing strategies adopted, the time step size, differencing schemes employed to transient and convective terms, and so on.

Table 3. Verification of mean Nusselt number and flow quantities with the available literature values for different Re numbers.

		Nu	Relative Error %	$C_{D,mean}$	Relative Error %	St	Relative Error %
Re=100	Present	5.626		1.722		0.1953	
	Chatterjee and Mondal (2015)	5.6932	1.19	1.7546	1.89	0.1926	1.38
	Dhiman and Shyam (2011)	5.5843	0.74	1.7316	0.56	0.1916	1.89
	De and Dalal (2007)			1.7607	2.25	0.1982	1.48
	Zeitoun et al. (2011)	5.557	1.23				
	Dalal et al. (2008)	5.67	0.78				
Re=150	Present	7.175		1.874		0.2148	
	Chatterjee and Mondal (2015)	7.1534	0.30	1.9037	1.58	0.2029	5.54
	Dhiman and Shyam (2011)	7.0447	1.82	1.8937	1.05	0.2041	4.98
	De and Dalal (2007)			1.875	0.05	0.2015	6.19
	Zeitoun et al. (2011)	7.246	0.99				
	Dalal et al. (2008)	7.31	1.88				

Errors in quantity f evaluated as $f\% = (f_{present} - f_{literature}) / f_{present} \times 100$.

Table 4. Validation of Nu, CD,mean, and St with the available literature values for Re=100 and 150.

		Nu	Relative Error %	$C_{D,mean}$	Relative Error %	St	Relative Error %
Re=100	Present	5.576		1.662		0.2051	
	Rasool et al. (2015)	5.589	0.23	1.7	2.29	0.2036	0.73
	Srikanth et al. (2010)	5.562	0.25	1.671	0.54	0.2004	2.29
Re=150	Present	7.2		1.935		0.2344	
	Rasool et al. (2015)	7.161	0.54	2	3.36	0.2247	4.14
	Srikanth et al. (2010)	7.127	1.01	1.934	0.05	0.2212	5.63

Errors in quantity f evaluated as $f\% = (f_{present} - f_{literature}) / f_{present} \times 100$.

In Table 4, the mean Nusselt number, mean drag coefficient, and Strouhal number results of the validation study are presented for a blockage ratio of BR=0.25 in Re=100 and 150. The velocity profile of the inlet is parabolic in this comparative study. This numerical investigation also depicts a good agreement. The minor variations in the results of Tables 3 and 4 can be explained by the size of the computational domain, meshing type and strategy, selection of convergence criteria, and so on.

RESULTS AND DISCUSSION

The effect of blockage ratio on the flow field and heat transfer in confined (BR=0.5, 0.25, 0.2, 0.1, 0.05, and 0.0333) and unconfined (BR=0.0143) channels where the fluid is water (Pr=7) is examined for Re=100, 150, and 200 and the Richardson number ranging from $-2 \leq Ri \leq 2$.

Investigation of the characteristics of flow and dimensionless temperature patterns

Seven cases of blockage ratios (BR=0.5, 0.25, 0.2, 0.1, 0.05, and 0.0333) and unconfined flow (BR=0.0143) are examined to observe their effects on the flow and heat transfer parameters. The iso-vorticity contours are presented in black lines whereas the the dimensionless temperature field is plotted only in brown color contours for temperatures above $\Theta \geq 0.1$) for a better depiction of cold and hot regions. The figures are intended to give an idea of how the flow evolves. The iso-vorticity contour labels (which scale differently for each case) condensed near the cylinder make the figures incomprehensible. However, the legend for the dimensionless temperature is the same for all cases and it is provided in Fig. 3 only to save printing space (Fig. 3 is cited for the legends in the other figures).

For BR=0.5, the iso-vorticities contours (black lines) superimposed on the dimensionless temperature field for Ri=-2, 0, 2, and Re=100 and 200 are shown in Fig. 3. The case of Ri=0 corresponds to pure forced convection from the cylinders. The vortex is regular at Re=100 and interacts with the boundary layer on the channel walls. In particular, when Ri=2, these vortex forms are seen to be more erratic. The assisting flow—natural and forced convection—being in the same direction weakened the vortex structure at a low Reynolds number. It is seen from Fig. 3 that the wake structure for Re=100 is significantly different from that for Re=200. The reason for the difference in this flow structure is the increasing inertia force with the increase in the Reynolds number. In Re=200, the dimensionless temperature field and iso-vorticity contours for all Ri numbers have shown similar characteristics, and in all cases, tightly-packed iso-vortices along the channel.

The instantaneous iso-vorticity contours and the dimensionless temperature field for BR=0.2, Ri=-2, 0, 2, and Re=100 and 200 obtained from the computations are given in Fig. 4. It is seen that the vortices do not interact with the boundary layer on the channel walls. Compared to Fig. 3, the reduction in the blocking ratio (widening the channel) leads to a larger vortex shedding period.

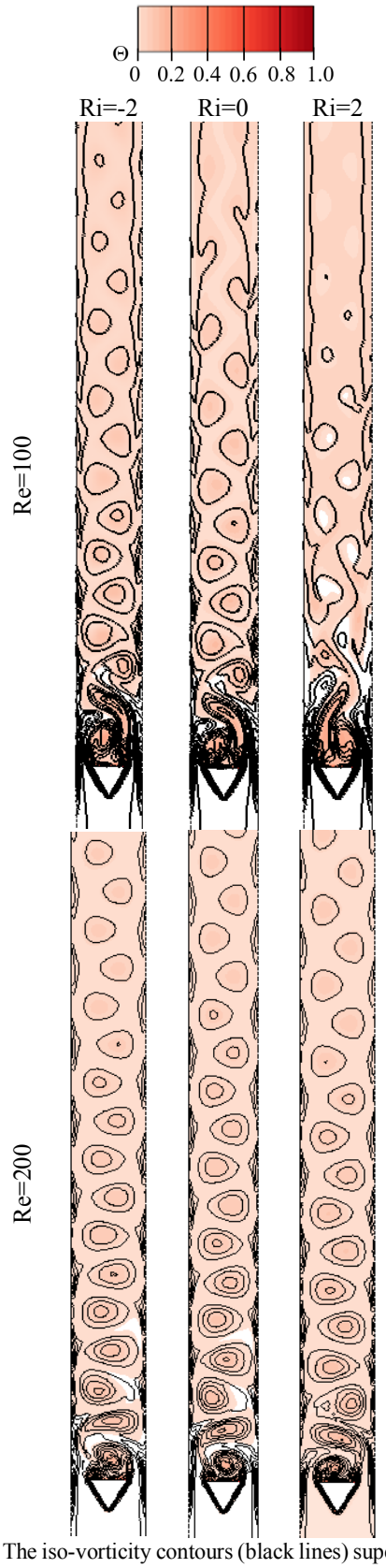

Figure 3. The iso-vorticity contours (black lines) superimposed with the dimensionless temperature field with different Ri and Re numbers for BR=0.5.

In the downstream area, the single-row closed vortex is formed behind the triangular cylinder. These iso-vortices are uniform and periodic in each case. In addition, the dimensionless temperature field near the cylinder walls is stacked very close to the walls, indicating that the temperature gradient is large.

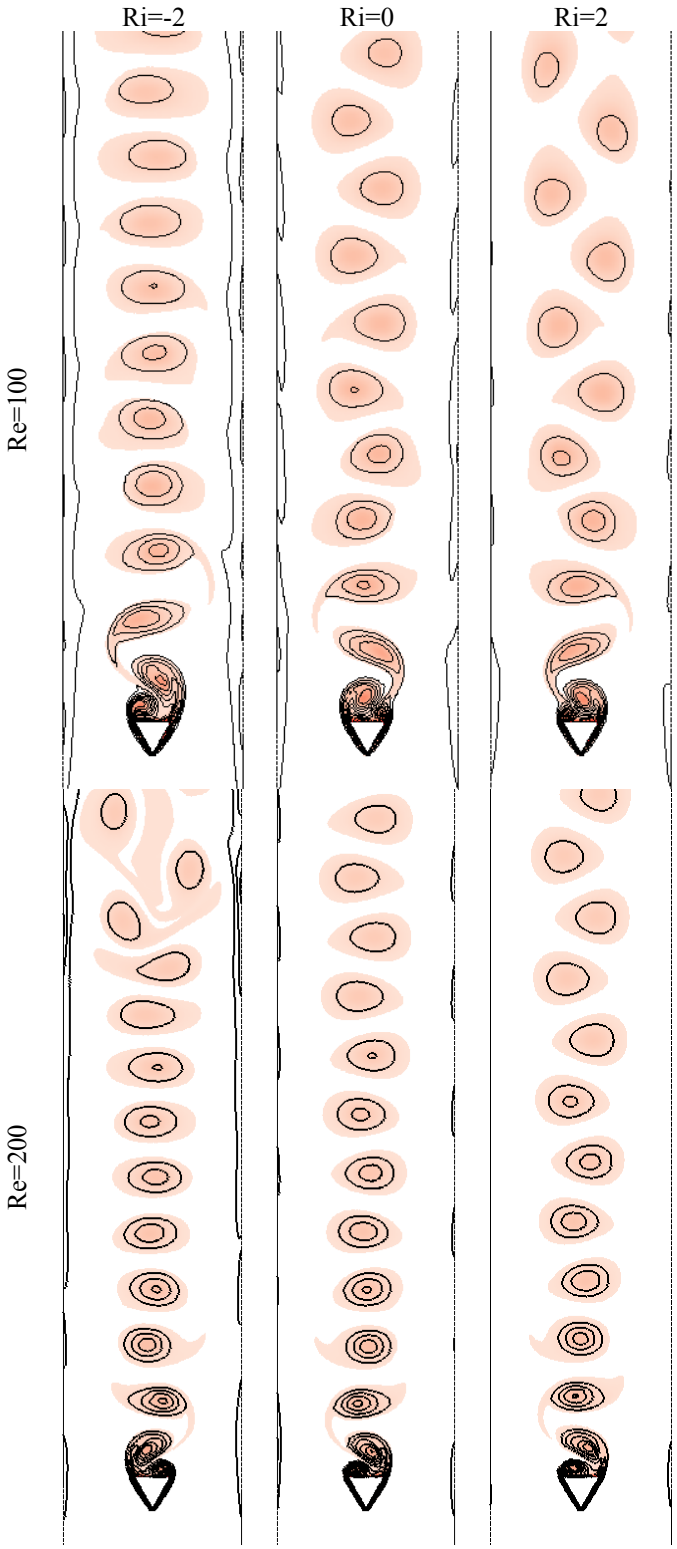

Figure 4. The iso-vorticity contours (black lines) superimposed with the dimensionless temperature field with different Ri and Re numbers for BR=0.2.

The variation of instantaneous iso-vorticity contours superimposed on the dimensionless temperature field for BR=0.1, Ri= -2, 0, 2, and Re=100 and 200 is shown in Fig. 5. In the Ri=-2 case, the vortices separated on the cylinder surface form two separate vortex columns after a certain distance, about *6D*, at both Re numbers. With increasing flow velocity at Re=200, two separate vortices occur closer to the cylinder (≈*4D*). At Ri=0 and Re=100, the double rows of round vortices formed behind the cylinder stretch out and tend to converge in the downstream direction. At Re=200, the double-column vortex structure is disrupted to form a single vortex structure in the downstream region. In the case of Ri=0 and Re=200, it is noted that the flow separation moves closer to the back of the cylinder. Natural convection, in the direction supporting forced convection, at Re=200 and Ri=2, the vortices behind the cylinder converged towards the center of the channel at about *7D*, yielding a single vortex column. In addition, the period of the vortices is slightly higher than that for Ri=-2 due to aiding natural convection.

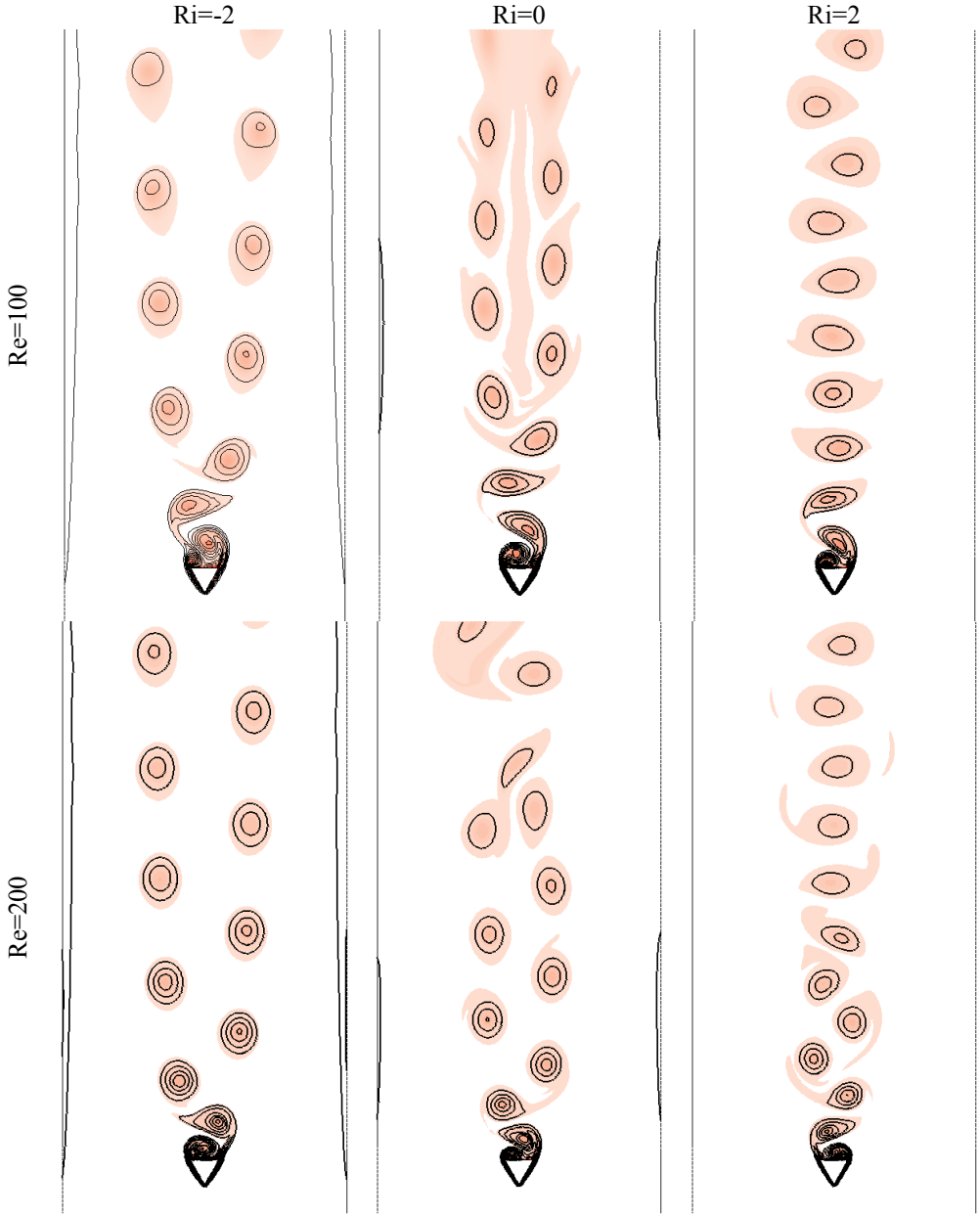

Figure 5. The variation of instantaneous iso-vorticity contours superimposed on the dimensionless temperature field (same legend as that of Figure 3) with different Ri and Re numbers for BR=0.1.

The variation of instantaneous iso-vorticity contours superimposed on the dimensionless temperature field for BR=0.033, Ri=-2, 0, 2, and Re=100 and 200 is illustrated in Fig. 6. For BR=0.033, the cylinder was away from the channel walls (H=30*D*), therefore vortex formation is not effected by the walls in all Re and Ri cases. Therefore, the channel walls are not shown in Fig. 6.

With the increasing Re number in Ri=-2, two separate vortices are formed behind the cylinder closer to the cylinder. Because of the downwards buoyancy force, the natural convection has a greater effect on the flow. Since the inertia force increases with Re = 200, the vortex shedding behind the cylinder is previously separated.

Initially, two distinct vortex columns are formed at about 11*D* distance behind the cylinder at Ri=0 and Re=100. However, the vortex columns stretch out as they tend to approach each other. At Re=200 and Ri=0, the vortices formed a non-uniform vortex trace. This situation is similar for Re=200.

Figure 7 illustrates the instantaneous iso-vorticity contours superimposed on the dimensionless temperature field in the unconfined channel (BR=0.0143) for Re=100, 200, and Ri=-2, 0, 2. For an unconfined channel and opposing buoyant flow (Ri=-2), it is seen that the wake behind the cylinder does not interact with the side walls, and the the dimensionless temperature field and iso-vorticities are able to spread out wider as it travels downwards along the channel. In both Reynolds cases, the formation of two vortices behind the cylinders is evident, and the two-column vortex structure is formed and maintained.

In pure forced convection (Ri=0), the formation of a two-column vortex street behind the cylinder dissolves further in the downstream region. Especially in Re = 200, the vortices in the left and right columns merge and turn into a single vortex street in the further downstream region. In Re=100, the two column vortex streets approach the channel center.

For the aiding buoyant flow case (Ri=2), a single von Karman vortex street appears instead of the two-column street for both Re cases. In Re=200, each vortex is lined up one after the other, whereas in Re=100, a single vortex column tends to diverge into two columns at about 14*D*. In addition, while the boundary layer formed around the cylinder at the same Reynolds numbers is thicker at Ri=-2, the boundary layer becomes thinner with increasing Ri numbers due to the direction of the fluid flow. As the first boundary layer separation takes place at about a 4*D* distance behind the cylinder for Ri=-2, this distance is 1*D* for Ri=2.

Consequently, the period of vortex shedding from an equilateral triangle cylinder decreases with increasing the Richardson number.

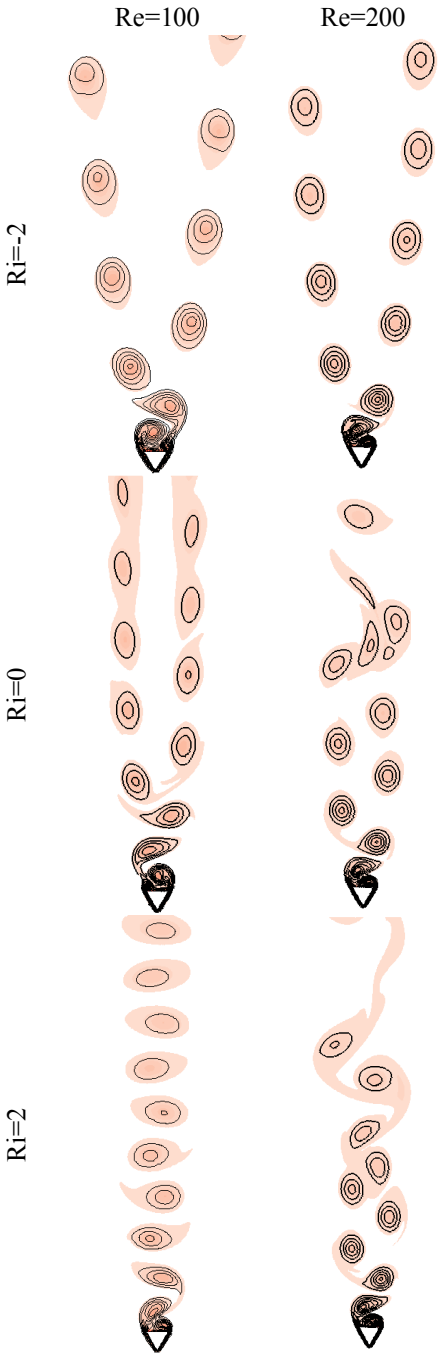

Figure 6. Variation instantaneous iso-vorticity contours superimposed on the dimensionless temperature field (same legend with that of Figure 3) with different Ri and Re numbers for BR=0.033.

Investigation of the flow and heat transfer coefficients

In Fig. 8, the variation of the average drag coefficient on the triangular cylinder with the blockage ratio and Richardson number is presented for Re=100 and 200. For all Reynolds and Richardson numbers, the average drag coefficient is the largest for BR=0.5 and the lowest in unconfined case. It is noted here that the average velocity at the center of the cylinder in the unconfined channel is 1 m/s, while the velocity at the center of the channel in the confined channel is 1.5 m/s. This causes the mean drag coefficient in the unconfined channel to be lower.

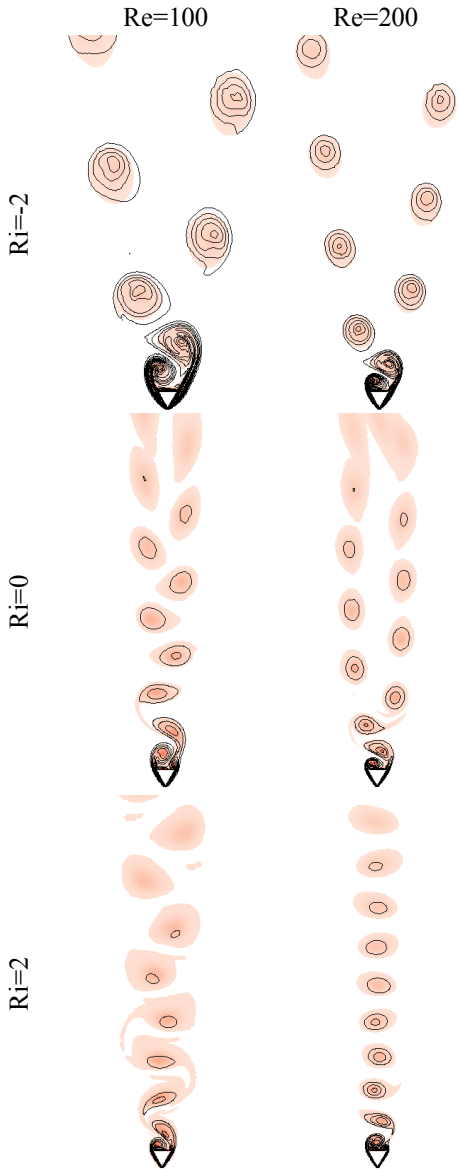

Figure 7. Variation instantaneous iso-vorticity contours superimposed on the dimensionless temperature field (same legend with that of Figure 3) with different Ri and Re numbers for the unconfined channel.

At Re=100, the mean C_D coefficient is close at all blocking ratios except for BR=0.5 and unconfined cases. The sudden decrease in the C_D coefficient at Re=100 and Ri=2 is attributed to the increasing effect of buoyancy, leading to a weakening of the vortex shedding (see Fig. 3). At Re=200, the mean C_D coefficient increases linearly with increasing Ri number and BR. Since the Richardson number gives the relative importance of buoyancy, the effect of buoyant flow becomes more pronounced, resulting in an increase in drag. In addition, the change in C_D with respect to the blockage ratio is more evident, especially at high Re numbers. For example: At Ri=-2, the drag coefficients of BR=0.25—with respect to the BR = 0.05 case—are about 36% and 61% larger for Re= 100 and 200, respectively. At Ri=2, the drag coefficients of BR=0.25–with respect to the BR=0.05 case–are about 5% and 17% larger for Re= 100 and 200, respectively. Teixeira et al. (2018) reported that the structural design application is important for the evaluation of design in external convective flows. According to the results obtained in this study, the blockage ratio is an important parameter in mixed heat transfer. The fluid undergoes convective acceleration in the region between the walls and the cylinder. For an increasing blockage ratio, the velocity gradient in the channel near the cylinder walls increases which, in turn, results in an increase in the viscous force acting on the cylinder and causes the drag coefficient to increase and delay the boundary layer separation.

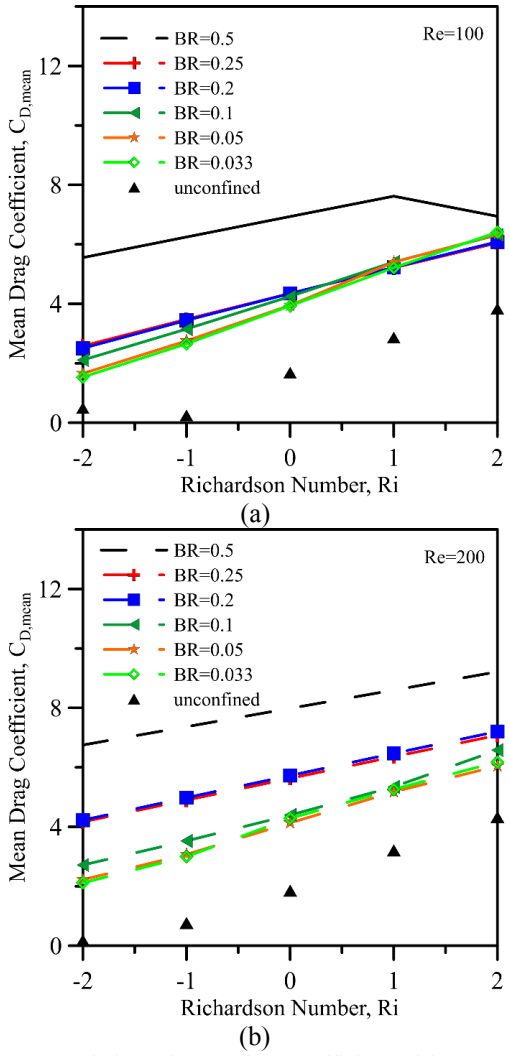

Figure 8. Variation of mean drag coefficient with (a) Re=100 and (b) Re=200 at various Richardson numbers and the blockage ratio.

The effect of Richardson number on $C_{L,rms}$ of various BR values is shown in Fig. 9 for Re=100 and 200. For both cases, the variation of $C_{L,rms}$ with Richardson number exhibits similar behavior, which increases with increasing Reynolds number. This outcome is attributed to the flow pattern in the downstream region. We also note that $C_{L,rms}$ also increases with increasing BR. At large BR ratios, the smaller the spacing between the channel walls, the stronger vortices that form behind the cylinder, resulting in a larger amplitude oscillation of the lift coefficient.

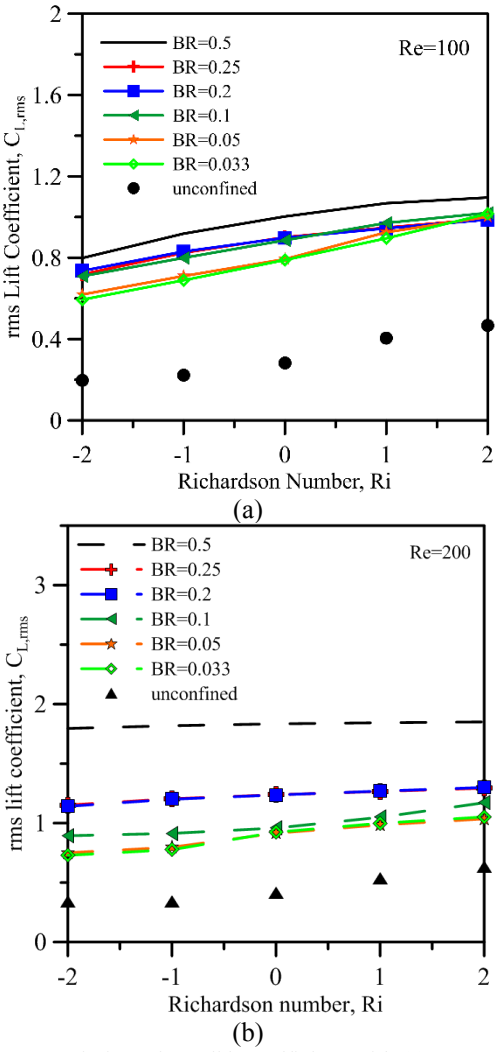

Figure 9. Variation of rms lift coefficient with (a) Re=100 and (b) Re=200 at various Richardson numbers and the blockage ratio.

Figure 10 shows the effect of the BR over the Strouhal number for Re=100 and 200. In the presence of a block effect, the St number varied in the range of about 0.22-0.47. On the other hand, in the unconfined channel, the St number is around 0.1-0.25. As can be seen from the vortex structure and the dimensionless temperature field in this study, the shedding of vortices develops behind the triangular cylinder. While the Strouhal number takes its maximum value in the narrowest channel configuration, it becomes minimum in unconfined flow cases. In unconfined channels, the vortices are formed as a result of the interaction of the inertial and buoyant forces. In this case, too, the effect of increasing the Richardson number (i.e., buoyancy) shows a significant change in the Strouhal number. As Sharma and Eswaran (2005) noted, the aiding flow (Ri>0) accelerates both the cylinder's boundary layers and the iso-vorticity shedding process, while opposing flow (Ri<0) slows it down and inhibits the shedding process. As a result, the Strouhal number also increases approximately linearly with the Richardson number for unconfined channels. However, the variation of the Strouhal number with the variation of the Richardson number in confined channels is relatively less compared to the unconfined channel. At Re=200, the St numbers are higher than Re=100. In addition, it is observed that the St numbers are very close to each other at BR=0.05 and BR=0.033 values in both Re numbers, where the blocking rate is small.

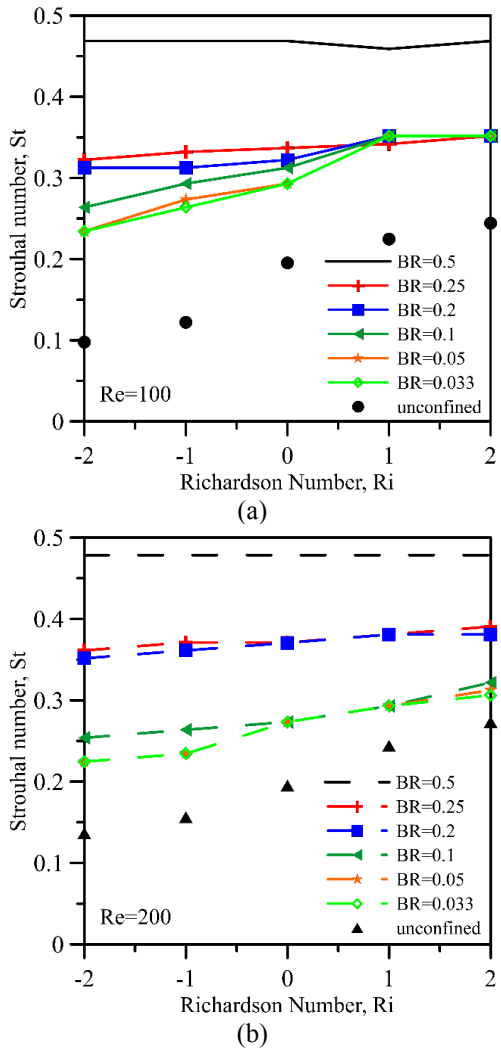

Figure 10. Variation of Strouhal number with (a) Re=100 and (b) Re=200 at various Richardson numbers and the blockage ratio.

Figure 11 shows the mean Nusselt number variations with the Richardson number and the blockage ratio for Re=100 and Re=200. A mean Nusselt number represents the heat transfer through a fluid layer as a result of convection relative to conduction across the same fluid layer. It is a dimensionless number usually derived from experimental or analytical and/or numerical studies, and it is often used in thermal engineering design calculations to estimate the convective heat transfer rates. The mean Nusselt number increases with an increase in the Reynolds number, as usual for all blockage ratios. Furthermore, the increase in the Nusselt number with the blocking rate is more pronounced at Re=200. For example, for Re=100, the mean Nusselt number for the case of BR=0.1 with respect to BR=0.033 depicts an increase of 4.67%, 3.35% and 3.86% for Ri=-2, 0 and 2, respectively. But in the case of BR=0.1 with respect to BR=0.033, the increase in the mean Nusselt number for Re=200 is 13%, 13.48% and 16.32% for Ri=-2, 0, and 2,

respectively. This is because, similar to the study done by Gandikota et al. (2010), as the blockage ratio increases, the shedding frequency of vortices increases, which in turn increases he heat transfer rate.

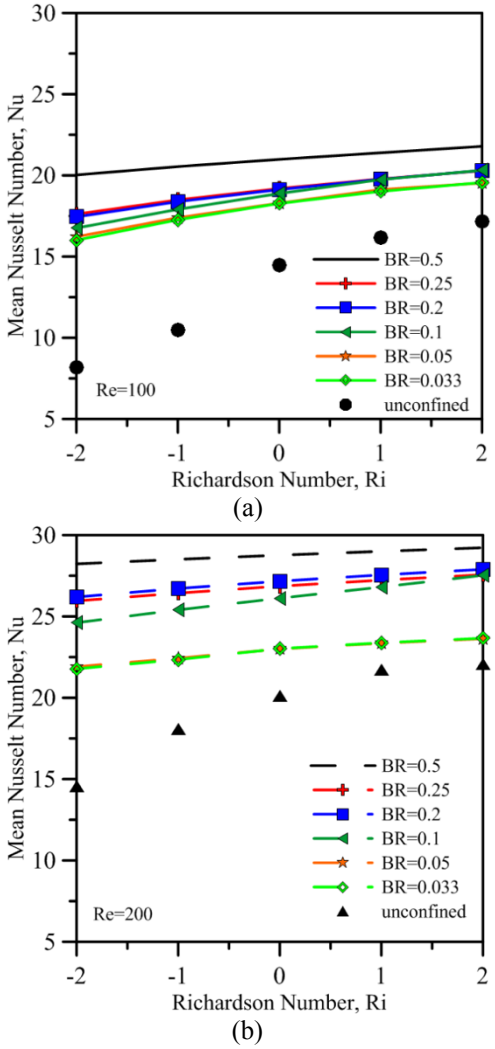

Figure 11. Comparison of the mean Nusselt number for different Richardson number and the blockage ratio at Re=100 (a) and Re=200 (b).

Note that the mean Nusselt number increases with increasing Richardson number due to the fact that the forced convection aids the natural convection transfer for Ri>0 and the forced convection constraints the natural convection transfer for Ri<0. In the unconfined channel case, higher Re and Ri numbers, which increase the effects of both buoyancy and inertia forces, result in a significant increase in the mean Nu number. For an unconfined channels, the average slope of the lines is 2.25 and 2.7 for Re=100 and 200, respectively. On the other hand, for BR=0.1, the average slope of the lines is 0.89 and 0.73 for Re=100 and 200, respectively. This shows that the Richardson number is a more important parameter for unconfined channel.

When the boundary layer around the cylinder is examined for the unconfined channel, we see that the boundary layer developed over the cylinder is thicker for Ri=-2, while the boundary layer formed around the cylinder decreases with the increase in the Ri number (see Fig. 7). As the temperature gradient increases, heat transfer also increases. In BR=0.5, the boundary layer around the cylinder is almost the same for all Ri numbers (see Fig. 3). Thus, it proves that the mean Nusselt number has not changed with Ri numbers.

The cases with maximum and minimum heat transfer rates are observed in BR=0.5 and unconfined flow cases, respectively. The local Nusselt number variations for these cases are depicted in Figure 12. The local Nusselt numbers (Nu_s) are plotted clockwise (0-1-2-3) in the direction along the periphery of the cylinders. In each case, the local Nusselt numbers reach their maximums at corners 1 and 2. The fluid, which encounters the fluid at the front corner (0-3), moves along the cylinder's side walls: 0-1 and 3-2. The local Nusselt number on these lateral walls (0-1 and 3-2) continues to increase towards the corners at 1 and 2. Since the system is symmetrical, the local Nusselt values between 0-1 and 3-2 are also symmetrical. The back (vertical) (from 1 to 2), on the other hand, is exposed to the slow-moving fluid, leading to a relatively slow moving vortex region, smaller temperature gradients, and local Nusselt number variations.

The local Nusselt number variation also changes with the Richardson number in both Reynolds numbers for the unconfined case. In the case of BR=0.5, it is observed that the local Nusselt number does not change significantly with the Richardson number in both cases where the inertia forces increased. The similarity and closeness of the local Nusselt number (seen in Figure 12) support the similarity of the boundary layers.

Correlations for flow characteristics and heat transfer

To the best of our knowledge, no correlation has been found in the literature for flow and heat transfer characteristics by combining the blocking ratio with the Reynolds and Richardson numbers. In this study, the drag/lift coefficients, Strouhal number, and mean Nusselt number for the range of $100 \leq Re \leq 200$, $-2 \leq Ri \leq 2$ have been computed for BR=0.5, 0.25, 0.2, 0.1, 0.05, 0.033, and 0.0143 (unconfined). Using the computed (observed) data, correlations for the mean drag and mean rms lift coefficients, Strouhal number, and mean Nusselt number have been developed.

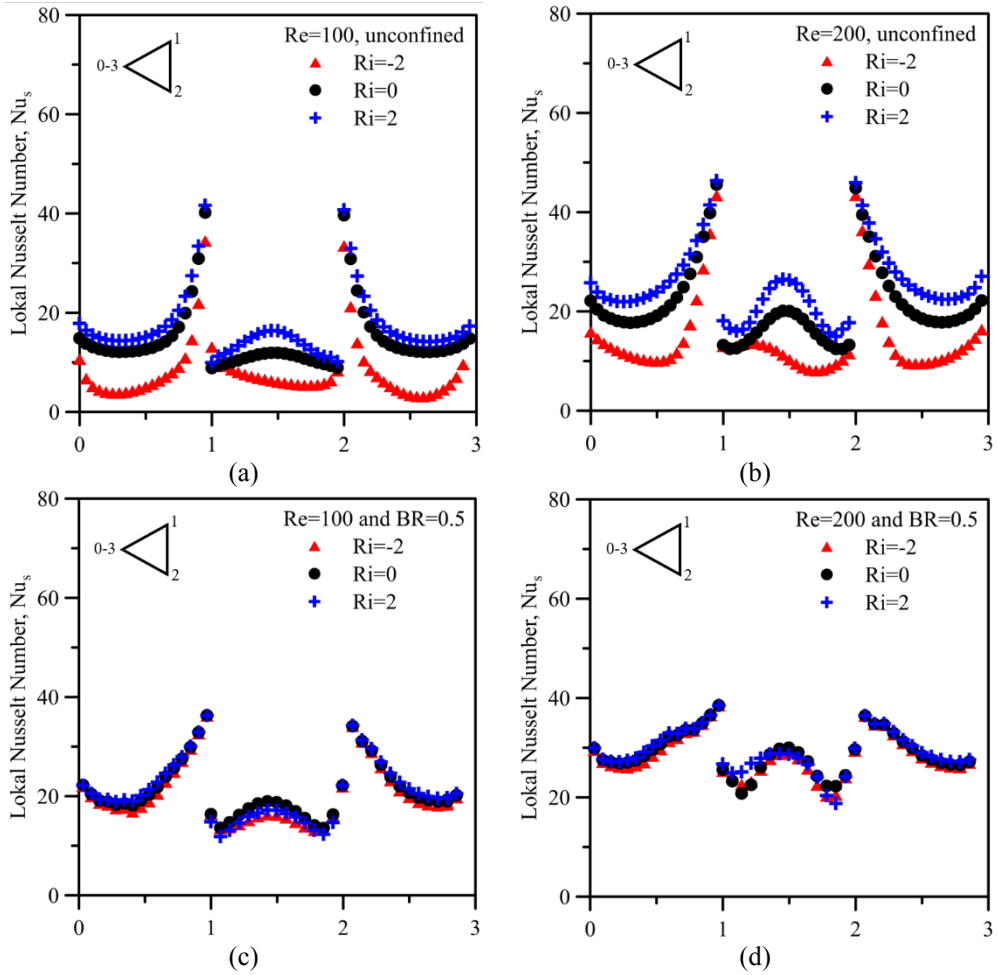

Figure. 12. Variation of time-averaged local Nusselt Number for a) Re=100 and unconfined channel, b) Re=200 and unconfined channel, c) Re=100 and BR=0.5, d) Re=200 and BR=0.5.

The mean computed drag coefficient over the equilateral-triangle cylinder surface area was compiled and used to obtain a non-linear regression. The mean drag coefficient correlation derived (prediction) is as follows:

$$C_{D,mean} = 3.3326\,\mathrm{Re}^{0.22}\left(-0.2074 + 0.091\mathrm{Ri} + \mathrm{BR}^{0.182}\right)$$
$$r^2 = 0.9804 \qquad (7)$$
$$100 \le \mathrm{Re} \le 200, -2 \le \mathrm{Ri} \le 2, 0.5 \le \mathrm{BR} \le 0.0143$$

We note that the r-squared value for the correlation is excellent. The mean drag coefficient increases with increasing blockage ratio, Reynolds, and Richardson numbers. According to the Eq. 7, the most dominant term is the Ri number. The plots of predicted (computed) data versus observed (computed) data provide both qualitative and quantitative information about how the curve fits. The consistency and model bias are described by the slope (m) and intercept (b) of the Predicted-Observed (PO) line, $C_{D,observed} = b + mC_{D,predicted}$, respectively. The resulting PO plot should be exactly aligned on the diagonal (i.e., y=Y line with rms=0) for identical observations/predictions. Similarly, data points that are near the diagonal line (normally, rms≠0) suggest that the entire data is reasonably well suited. All the drag coefficient PO data was additionally fitted to a linear curve, yielding the following results: $-0.000147831 + 0.999972x$. The linear relationship between $C_{D,observed}$ and $C_{D,predicted}$ is validated by the slope of m=0.999972 (approaching unity). Any deviation of the slope from unity indicates a relative scaling factor between the two sets. A non-zero intercept indicates that the population is shifted by a constant offset relative to the other. The intercept of the correlation is very small (b=-0.0001478), so the model bias is negligible.

Similarly, using nonlinear regression, developed correlations for other flow characteristic properties, $C_{L,rms}$ and St, are presented as follows:

$$C_{L,rms} = 0.0456\,\mathrm{Re}^{0.5}\, e^{\left(1+0.0531\mathrm{Ri}+0.01955\mathrm{Ri}^2\right)}\,\mathrm{BR}^{0.2324}$$
$$r^2 = 0.9582 \qquad (8)$$
$$100 \le \mathrm{Re} \le 200, -2 \le \mathrm{Ri} \le 2, 0.5 \le \mathrm{BR} \le 0.0143$$

$$\mathrm{St} = 0.354\,\mathrm{Re}^{0.027}\left(0.396 + 0.047\mathrm{Ri} + \mathrm{BR}^{0.443}\right)$$
$$r^2 = 0.9903 \qquad (9)$$
$$100 \le \mathrm{Re} \le 200, -2 \le \mathrm{Ri} \le 2, 0.5 \le \mathrm{BR} \le 0.0143$$

The lift rms coefficient changes drastically with the Reynolds and Richardson numbers, and the Strouhal number also varies greatly with the blockage ratio. For these correlations, all rms lift coefficient and St numbers PO data are also fitted to linear curves, which yielded $C_{L,rms,observed} = -0.01195 + 1.01164 C_{L,rms,predicted}$ and $St_{observed} = 0.0001279 + 0.999626\,St_{predicted}$, respectively.

Early experimental studies involving forced flows for the flow characteristics and the Nusselt numbers were usually expressed (due to the nonlinear nature of flow and transfer) by a simple power-law model where the Re number was the main independent variable; that is, $Nu = C\,Re^n\,Pr^m$ (Bergman et al., 2018). To determine the variation with the Richardson number, the graph of Nu_{mixed} / Nu_{forced} ratio is examined. The plot of this ratio reveals the magnitude and behavior of the deviations from that of the forced convection due to natural convection effects (i.e., Ri number). The effect of BR was also observed in the same manner, and the general form of a correlation was assumed to be in the form $C\,Re^n f(Ri,BR)$, where $f(Ri,BR)$ is a function determined by visual inspection of Nu_{mixed} / Nu_{forced} ratio and trial-and-error that minimized the sum of squares and maximizes r^2. It has been observed that the Nusselt number varies linearly with the Richardson number while exponentially with the BR ratio. This strategy has been employed in the literature to determine the effect of parameters other than Reynolds and Prandtl numbers (Chen et al., 1986; Lin et al., 1990; Altaç and Altun, 2014; Dalkilic et al., 2019).

Using a nonlinear regression model that minimizes the sum of the squares of the errors for the mean Nusselt numbers collected from the cylinder surface area leads to

$$Nu = 2.858\,Re^{0.449}\left(1 + 0.0356\,Ri\right)BR^{0.092}$$
$$r^2 = 0.99603 \qquad (10)$$
$$100 \le Re \le 200, -2 \le Ri \le 2, 0.5 \le BR \le 0.0143$$

To assess the accuracy of the correlation, the Nusselt number obtained by the proposed correlation against the Nusselt number calculated by numerical simulation. The linear curve for the Nusselt number is $Nu_{observed} = -0.25642 + 1.01149 Nu_{predicted}$. The model is consistent since the slope is very close to 1 (i.e., 45 degree inclination), and the intercept is -0.25642, which is a very small deviation, considering the average value of the mean Nusselt number is 21.6701. Figure 13 depicts visually the Predicted-Observed plots of correlations for (a) the mean drag coefficient, (b) rms lift coefficient, (c) Strouhal number, (d) Nusselt number. It should be noted that the data for all the Nusselt and Strouhal numbers and the mean drag coefficient spread well around the best curves fit, which is supported with r-squared values of greater than 0.98.

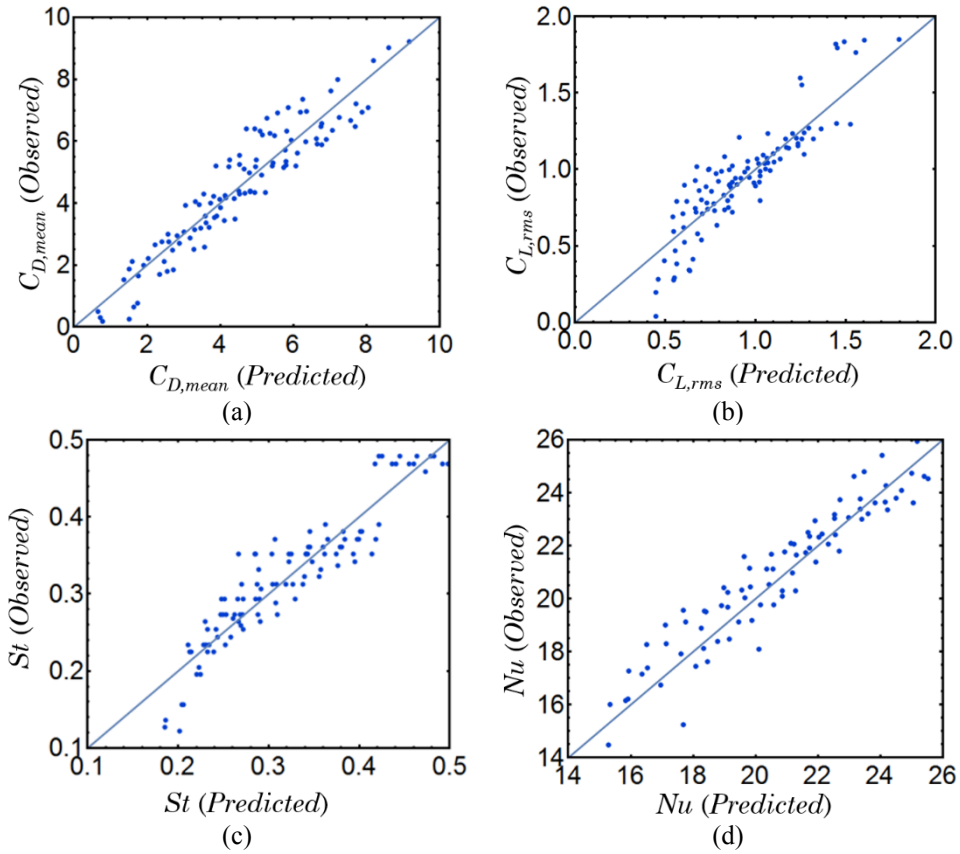

Figure 13. The Predicted-Observed plots of correlations for (a) the mean drag coefficient, (b) rms lift coefficient, (c) Strouhal number, (d) Nusselt number.

CONCLUSION

In this study, two-dimensional mixed heat transfer (transient forced convection and natural convention) and fluid flow over equilateral triangular cylinders in confined and unconfined channels are performed numerically. Three dimensionless parameters (Blockage Ratio, Reynolds, and Richardson numbers) implemented in the new correlations considered the influence of mixed convective heat transfer (i.e., Nu) and flow (i.e., $C_{D,mean}$, $C_{L,rms}$, and St). Five Richardson numbers (Ri=-2, -1, 0, 1, and 2), three Reynolds numbers (Re=100, 150, and 200), and seven blockage ratios (BR=0.5, 0.25, 0.2, 0.1, 0.05, 0.0333 for confined channels and 1/70 for unconfined channels) are investigated. The results obtained from this study are summarized below.

- When the blockage ratio increases, the boundary layer of the channel wall and the vortex behind the cylinder interact in the downstream region. Thus, the vortices formed behind the cylinder at the decreasing blockage ratio can be spread to the channel.
- With decreasing blockage ratios, a two-column vortex was observed at Ri=0 and Ri=-2. A single vortex form is formed when natural convection supports forced convection (Ri=2). This is due to the fact that the boundary layer around the triangular cylinder is thinner compared to Ri=0 and Ri=-2.
- In the presence of a strong buoyant forces, the flow field is significantly altered. The density difference causes hot fluid to be discharged into the near wake region, increasing the mass moving underneath the cylinder and affecting the flow field. While examining the iso-vorticity contours and the dimensionless temperature field for the unconfined channel, it is seen that the frequency of the vortices increases with the increasing Richardson number due to aiding natural convection.
- In all Reynolds and Richardson numbers, the drag coefficient and the mean Nu number are the lowest in the case of the unconfined channel and the highest in the severely confined BR=0.5 case. In addition, at high Reynolds numbers, both the drag coefficient and the mean Nu number are affected largely by the blockage ratio. For Ri=0, the drag coefficients of BR=0.25–with respect to the BR=0.05 case–are about 9% and 29% larger for Re= 100 and 200, respectively.
- Any flow characteristic's rms value serves as a gauge for fluctuations in that specific flow characteristic. However, the Reynolds and Richardson numbers for which the Re-Ri domain for the lift coefficient was created also influence these oscillations. The $C_{L,rms}$ value tends to increase as the Reynolds and Richardson numbers increase. However, the $C_{L,rms}$ value is more affected by the change in the BR. At high BR ratios, stronger vortices develop behind the cylinder due to the narrower channel wall spacing, which leads to a lift coefficient oscillation with a bigger amplitude. However, in cases where BR is high, $C_{L,rms}$ does not change much with the change in the Richardson number due to the dominance of inertia forces at high Reynolds numbers. At BR=0.5, the $C_{L,rms}$ of Ri=2 relative to Ri=-2 are greater than 37.283% and 3.067% at Re=100 and 200, respectively.
- The mean Nusselt increases with Re number and BR, as well as Ri number, due to buoyancy-induced effects of the flow field. The mean Nusselt number of BR=0.5 and Ri=-2 is about 2.5-2 times that of the unconfined channel and R=-2, and the mean Nusselt number of BR=0.5 and Ri=2 is about 1.22-1.15 times that of the unconfined channel and Ri=2.
- For small blockage rates, the Strouhal number increases with increasing Ri number, whereas it is almost the same with increasing Ri number for BR=0.5. The minimum value of the Strouhal number is obtained at an unconfined channel, and the maximum value is obtained at BR=0.5.
- As demonstrated, the correlations developed by nonlinear regressions achieve good prediction capability for mixed convection heat transfer and fluid flow from a triangular cylinder in a vertical channel.

NOMENCLATURE

A	surface area [m^2]
BR	blockage ratio defined as D/H [-]
C	coefficient
D	side lenght of equilateral triangular cylinder [m]
F	force [N]
g	acceleration of gravity
g	dimensionless gravity
Gr	Grashof number [-]
H	channel width [m]
h	mean heat transfer coefficient [$W/m^2 \cdot K$]
k	thermal conductivity [W/m·K]
Nu	mean Nusselt number [-]
$\bar{P}$	pressure [N/m^2]
P	dimensionless velocity components [-]
Pr	Prandtl number [-]
Ri	Richardson number [-]
Re	Reynolds number [-]
T	temperature [K]
t	time
$\bar{u}, \bar{v}$	velocity components [m/s]
u, v	dimensionless velocity components [-]
$\overline{U}$	mean velocity components [m/s]

$\bar{x}, \bar{y}$ cartesian coordinate system [m]
x, y dimensionless cartesian coordinates [-]

Greek Symbol
α thermal diffusivity [m^2/s]
β thermal expansion coefficient [K^{-1}]
μ dynamic viscosity [$N \cdot s/m^2$]
υ kinematic viscosity [m^2/s]
ρ density [kg/m^3]
Θ dimensionless temperature [-]
τ dimensionless time [-]

Subscripts
D drag
L lift
w wall
∞ free stream property

References

Abbassi, H., Turki, S., and Nasrallah, S. B., 2001, Mixed convection in a plane channel with a built-in triangular prism, *Numerical Heat Transfer, Part A: Applications: An International Journal of Computation and Methodology* 39: 307–320.

Akbari, M., Lavasani, A. M. and Naseri, A., 2021, Experimental investigation of the heat transfer for non-circular tubes in a turbulent air cross flow, *Experimental Heat Transfer* 34 (6): 531-530.

Altaç Z. and Altun, Ö., 2014, Hydrodynamically and thermally developing laminar flow in spiral coil tubes, *International Journal of Thermal Sciences* 77: 96-107.

Altaç, Z., Sert Z., Mahir, N., and Timuralp, Ç., 2019, Mixed convection heat transfer from a triangular cylinder subjected to upward cross flow, *International Journal of Thermal Sciences* 137: 75-85.

Ali, M., Zeitoun, O., and Nuhait, A., 2011, Forced convection heat transfer over horizontal triangular cylinder in cross flow, *International Journal of Thermal Sciences* 50: 106–114.

Arif, M. R. and Hasan, N., 2020, Large-scale heating effects on global parameters for flow past a square cylinder at different cylinder inclinations, *International Journal of Heat and Mass Transfer* 161: 120237.

Barati, E., Biabani, M. and Zarkak, M. R., 2022, Numerical investigation on vortex-induced vibration energy harvesting of a heated circular cylinder with various cross-sections. *International Communications in Heat and Mass Transfer* 132: 105888.

Bergman, T. L., Lavine, A. S. and Incropera, F. P., and DeWitt, D. P., 2018, Fundamentals of Heat and Mass Transfer, Wiley (WileyPLUS Products); 8th edition, Table 7.7, page 447.)

Bovand, M., Rashidi, S., Esfahani, J.A., 2015, Enhancement of heat transfer by nanofluids and orientations of the equilateral triangular obstacle, *Energy Conversion and Management* 97: 212-223.
Camarri, S., Salvetti, M. V., and Buresti, G., 2006, Large-eddy simulation of the flow around a triangular prism with moderate aspect ratio, *Journal of Wind Engineering and Industrial Aerodynamics* 94: 309-322.

Chatterjee, D., and Mondal, B., 2015, Mixed convection heat transfer from an equilateral triangular cylinder in cross flow at low Reynolds numbers, *Heat Transfer Engineering* 36 (1): 123–133.

Chattopadhyay, H., 2007, Augmentation of heat transfer in a channel using a triangular prism, *International Journal of Thermal Sciences* 46: 501-505.

Chen T. S., Armaly, B. F., Ramachandran, N., Correlations for laminar mixed convection flows on vertical, inclined, and horizontal flat plates, *Journal of Heat Transfer*, 108, 835-840.

Çelik, Z., Altaç, Z., 2023, Numerical investigation of two-dimensional unsteady flow and heat transfer from rounded equilateral isothermal triangular cylinders in cross flow, *Ocean Engineering* 269: 113468.

Dalal, A., Eswaran, V., and Biswas, G., 2008, A finite-volume method for Navier-Stokes equations on unstructured meshes, *Numerical Heat Transfer, Part B: Fundamentals* 54 (3): 238–259.

Dalkilic, A. S., Çebi, A., Celen, A., 2019, Numerical analyses on the prediction of Nusselt numbers for upward and downward flows of water in a smooth pipe: effects of buoyancy and property variations, *Journal of Thermal Engineering*, 5 (3): 166-180.

De, A. K., and Dalal, A., 2006, Numerical simulation of unconfined flow past a triangular cylinder, *International Journal for Numerical Methods in Fluids* 52 (7): 801–821.

De, A. K., and Dalal, A., 2007, Numerical study of laminar forced convection fluid flow and heat transfer from a triangular cylinder placed in a channel, *ASME Journal of Heat Transfer* 129: 646–656.

Dhimana, A., and Shyam, R., 2011, Unsteady heat transfer from an equilateral triangular cylinder in the unconfined flow regime, *ISRN Mechanical Engineering* 932738: 1–13.

Dhiman, A. K., 2016, Flow and heat transfer phenomena around an equilateral triangular bluff body: effect of wall confinement, *Heat Transfer - Asian Research* 45: 608–630.

Dulhani, J. P., and Dalal, A., 2015, Flow past an equilateral triangular bluff obstacle: computational study of the effect of thermal buoyancy on flow physics and heat transfer, *Numerical Heat Transfer, Part A: Applications: An International Journal of Computation and Methodology* 67: 476–495.

El-Wahed, A. K., Johnson, M. W., and Sproston, J. L., 1993, Numerical study of vortex shedding from different shaped bluff bodies, *Flow Measurement and Instrumentation* 4: 233-240.

FLUENT 6.3.26 User's Guide, Fluent Inc., Lebanon, NH, 2007.

GAMBIT 2.2 User's Guide, Fluent Inc., Lebanon, NH, 2004.

Gandikota, G., Amiroudine, S., Chatterjee, D., and Biswas, G., 2010, The effect of aiding/opposing buoyancy on two dimensional laminar flow across a circular cylinder, *Numerical Heat Transfer, Part A: Applications: An International Journal of Computation and Methodology* 58: 385-402.

Hassab, M. A., Teamah, M. A., El-Maghlany, W. M., and Kandil, M. A., 2013, Experimental study for a mixed convection heat transfer from an isothermal horizontal triangular cylinder, *International Journal of Engineering Sciences* 6: 210–225.

Hyun, S., and SikYoon, N. H., 2022, Effect of the wavy geometric disturbance on the flow over elliptic cylinders with different aspect ratios, *Ocean Engineering* 243: 110287.

Laidoudi, H. and Bouzi, M., 2018, The effects of aiding and opposing thermal buoyancy on the downward flow around a confined circular cylinder, *Periodica Polytechnica Mechanical Engineering* 62 (1): 42-50.

Lin, H. T., Yu, W. S., Chen, C. C., 1990, Comprehensive correlations for laminar mixed convection on vertical and horizontal flat plates, *Wärme - und Stoffübertragung*, 25, 353-359.

Lupi, F., 2013, A new aerodynamic phenomenon and its effects on the design of ultra-high cylindrical towers, Chapter 3. Flow around circular cylinders: state of the art, *Ph.D. Thesis* University of Florence. (https://flore.unifi.it/retrieve/handle/2158/829166/

Mahir, N. and Altaç, Z., 2019, Numerical investigation of flow and combined natural-forced convection from an isothermal square cylinder in crossflow, *International Journal of Heat and Fluid Flow* 75: 103-121.

Patel, S. A. and Chhabra, R. P., 2019, Buoyancy-assisted flow of yield stress fluids past a cylinder: Effect of shape and channel confinement, *Applied Mathematical Modelling* 75: 892-915.

Peng, J., Fu, X. and Chen, Y., 2008, Experimental investigations of Strouhal number for flows past dual triangulate bluff bodies, *Flow Measurement and Instrumentation* 19: 350-357.

Rasool, T., Dhiman, A. and Parveez, M., 2015, Cross-buoyancy mixed convection around a confined triangular bluff body, *Numerical Heat Transfer, Part A: Applications: An International Journal of Computation and Methodology* 67: 454–475.

Salimipour, E., and Yazdani, S., 2022, Study on the fluid flow and heat transfer characteristics of a horizontal elliptical cylinder under thermal buoyancy effect, *International Journal of Heat and Mass Transfer* 192: 122948.

Shademani, R., Ghadimi, P., Zamanian, R. and Dashtimanesh, A., 2013, Assessment of air flow over an equilateral triangular obstacle in a horizontal channel using FVM, *Journal of Mathematical Sciences and Applications* 1: 12-16.

Sharma, A., and Eswaran, V., 2005, Effect of channel-confinement and aiding/opposing buoyancy on the two-dimensional laminar flow and heat transfer across a square cylinder, *International Journal of Heat and Mass Transfer* 48 (25-26): 5310-5322.

Sharma, K. R. and Dutta, S., 2022, Flow over a square cylinder at intermediate Reynolds numbers, *Journal of Fluids Engineering* 144 (12): 121303.

Srigrarom, S. and Koh, A. K. G., 2008, Flow field of self-excited rotationally oscillating equilateral triangular cylinder, *Journal of Fluids and Structures* 24: 750-755.

Srikanth, S., Dhiman, A. K. and Bijjam, S., 2010, Confined flow and heat transfer across a triangular cylinder in a channel, *International Journal of Thermal Sciences* 49: 2191–2200.

Teixeira, F. B., Lorenzini, G., Errera, M. R., Rocha, L. A. O., Isoldi, L. A., and dos Santos, E. D., 2018, Constructal Design of triangular arrangements of square bluff bodies under forced convective turbulent flows, *International Journal of Heat and Mass Transfer* 126: 521-535.

Tiwari, A. K., and Chhabra, R. P., 2014, Effect of Orientation on the Steady Laminar Free Convection Heat Transfer in Power-Law Fluids from a Heated Triangular Cylinder, *Numerical Heat Transfer, Part A: Applications* 65 (8): 780-801.

Varma, N., Dulhani, J. P., Dalal, A., Sarkar, S., and Ganguly, S., 2015, Effect of channel confinement on mixed convective flow past an equilateral triangular cylinder, *ASME Journal of Heat Transfer* 121013: 1-7.

Yagmur, S., Dogan, S., Aksoy, M. H., Goktepeli, I., and Ozgoren, M., 2017, Comparison of flow characteristics around an equilateral triangular cylinder via PIV and Large Eddy Simulation methods, *Flow Measurement and Instrumentation* 55: 23-36.

Zeitoun, O., Ali, M., and Nuhait, A., 2010, Numerical study of forced convection around heated horizontal triangular ducts, *Heat Transfer* 68: 201-212.

Zeitoun, O., Ali, M., and Nuhait, A., 2011, Convective heat transfer around a triangular cylinder in an air cross flow, *International Journal of Thermal Sciences* 50 (9): 1685-1697.

Zhang, N., Rong, L. W., Dong, K. J., and Zeng, Q. D., 2020, Fluid flow and heat transfer characteristics over a superelliptic cylinder at incidence, *Powder Technology* 360: 193-208.

Zhu, H., Tang, T., Zhou, T., Liu, H., and Zhong. J., 2020, Flow structures around trapezoidal cylinders and their hydrodynamic characteristics: Effects of the base length ratio and attack angle, *Physics of Fluids* 32: 1036061-22.

Zerrin SERT is an assistant professor at Eskişehir Osmangazi University. She received her M.Sc. and Ph.D. in mechanical engineering from Eskişehir Osmangazi University, Turkey. Her research area is CFD, forced convection, aerodynamics, radiation, and heat transfer.